Published in final edited form as:

Cell. 2016 April 7; 165(2): 434–448. doi:10.1016/j.cell.2016.02.009.

Kv3.3 channels bind Hax-1 and Arp2/3 to assemble a stable local actin network that regulates channel gating

Yalan Zhang[#1], **Xiao-Feng Zhang**[#3], **Matthew R. Fleming**[1], **Anahita Amiri**[4], **Lynda El-Hassar**[1], **Alexei A. Surguchev**[1], **Callen Hyland**[3], **David P. Jenkins**[1], **Rooma Desai**[1], **Maile R. Brown**[1], **Valeswara-Rao Gazula**[1], **Michael F. Waters**[7], **Charles H. Large**[8], **Tamas L. Horvath**[6], **Dhasakumar Navaratnam**[5], **Flora M. Vaccarino**[4], **Paul Forscher**[3,#], and **Leonard K. Kaczmarek**[1,2,#]

[1]Department of Pharmacology, Yale University School of Medicine, 333 Cedar Street, New Haven, CT 06520

[2]Department of Cellular and Molecular Physiology, Yale University School of Medicine, 333 Cedar Street, New Haven, CT 06520

[3]Department of Molecular, Cellular and Developmental Biology, Yale University School of Medicine, 333 Cedar Street, New Haven, CT 06520

[4]Department of Child Study Center and Neurobiology, Yale University School of Medicine, 333 Cedar Street, New Haven, CT 06520

[5]Department of Neurology, Yale University School of Medicine, 333 Cedar Street, New Haven, CT 06520

[6]Department of Comparative Medicine, Yale University School of Medicine, 333 Cedar Street, New Haven, CT 06520

[7]Department of Neurology, University of Florida College of Medicine, HSC Box 100236, Gainesville, FL 32610-0236

[8]Autifony Therapeutics Limited, Imperial College Incubator, Level 1 Bessemer Building, London, SW7 2AZ UK

[#] These authors contributed equally to this work.

Send correspondence to: Leonard K. Kaczmarek, Department of Pharmacology, Yale University School of Medicine, P.O. Box 208066, New Haven, Connecticut 06520-8066, leonard.kaczmarek@yale.edu, Paul Forscher, Department of Molecular, Cellular and Developmental Biology, P.O. 208103, Yale University, New Haven, CT 06520-8103, paul.forscher@yale.edu.
[#]Co-corresponding Authors

Author Contributions

YZ generated constructs, carried out all CHO cell patch clamp recordings and western blots. XFZ carried out all imaging experiments on CHO cells. MRF and DPJ did the label-free optical biosensor experiments. AA and FMV generated the iPSC cells. LEH did patch recording on brainstem neurons. AAS and DN did the yeast two-hybrid screen. CH did initial immunlocalization experiments. RD did immunostaining for Kv3.3 in brainstem slices. MRB. and VRG did initial western blotting and immunolocalization experiments. MFW and CHL generated constructs and cell lines for the human Kv3.3 channels. TLH did supporting experiments on Hax-1 localization. LKK and PF conceived the project and wrote the paper.

Abstract

Mutations in the Kv3.3 potassium channel (KCNC3) cause cerebellar neurodegeneration and impair auditory processing. The cytoplasmic C-terminus of Kv3.3 contains a proline-rich domain conserved in proteins that activate actin nucleation through Arp2/3. We found that Kv3.3 recruits Arp2/3 to the plasma membrane, resulting in formation of a relatively stable cortical actin filament network resistant to cytochalasin D which inhibits fast barbed end actin assembly. These Kv3.3-associated actin structures are required to prevent very rapid N-type channel inactivation during short depolarizations of the plasma membrane. The effects of Kv3.3 on the actin cytoskeleton are mediated by the binding of the cytoplasmic C-terminus of Kv3.3 to Hax-1, an anti-apoptotic protein that regulates actin nucleation through Arp2/3. A human Kv3.3 mutation within a conserved proline-rich domain produces channels that bind Hax-1 but are impaired in recruiting Arp2/3 to the plasma membrane, resulting in growth cones with deficient actin veils in stem cell-derived neurons.

Abstract

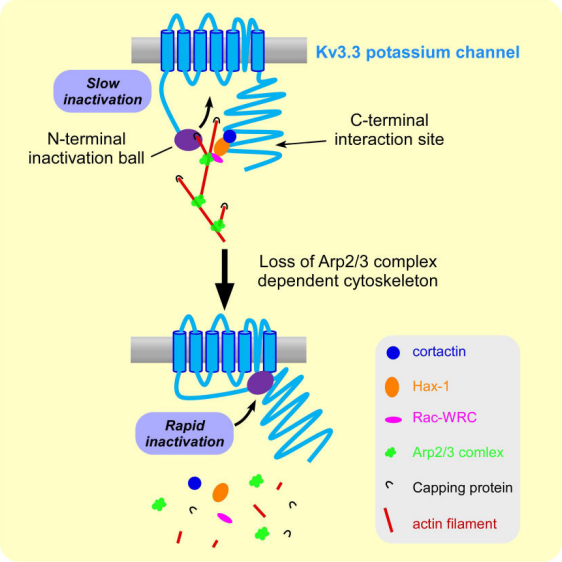

Introduction

The voltage-dependent Kv3.3 potassium channel is widely expressed in the nervous system, and is prominent in auditory brainstem nuclei and cerebellum, where neurons fire at rates of several hundred Hz. In the cerebellar cortex, high Kv3.3 expression is found in Purkinje cells (Chang et al., 2007; Sacco et al., 2006). Like other members of the Kv3 subfamily, such as Kv3.1, Kv3.3 channels activate and deactivate rapidly in response to changes in transmembrane voltage (Rudy and McBain, 2001). The major role of these delayed rectifier-type channels is to contribute to action potential repolarization. In response to sustained depolarization, Kv3.3 channels inactivate slowly over hundreds of milliseconds by an N-terminal ball-and-chain mechanism. This rate of inactivation can be further slowed by phosphorylation of two residues at the N-terminus by protein kinase-C (Desai et al., 2008).

Spinocerebellar ataxia type 13 (SCA13) is a human autosomal dominant disease caused by mutations in the *KCNC3* gene, which encodes the Kv3.3 channel. SCA13 patients have cerebellar atrophy and suffer motor symptoms (Waters et al., 2006; Zhang and Kaczmarek, 2015). Such mutations also severely impair localization of auditory stimuli (Middlebrooks et al., 2013). Some previously described Kv3.3 mutations that result in SCA13 are located in or close to transmembrane regions of the protein and suppress current either by altering channel gating or by acting as dominant negative subunits (Irie et al., 2014; Minassian et al., 2012; Waters et al., 2006). Although it is sometimes assumed that this disease is caused by the enhanced neuronal excitability resulting from suppression of potassium current, it is not clear why mutations in other channels that result in increased excitability and epileptic seizures are not associated with neurodegeneration, and why no neurodegenerative disease mutations have been found in other Kv3 family channels that have similar physiological roles. This suggests that Kv3.3 may have additional cellular functions distinct from regulation of excitability (Lee et al., 2014).

The very large size of the cytoplasmic C-terminal domain of Kv3.3 distinguishes it from other Kv3 subfamily channels, and suggests it has interactions with cytoplasmic signaling pathways and/or the cytoskeleton. We report that the Kv3.3 channel binds the anti-apoptotic protein Hax-1 to induce Arp2/3 (actin-related protein 2/3 complex) dependent actin filament nucleation at the plasma membrane. The resulting cortical actin filament network regulates the inactivation of Kv3.3. We also describe a Kv3.3 mutation, G592R that results in adult-onset SCA13. The G592R mutant is deficient in coordinating Arp2/3 dependent cortical actin assembly, resulting in neuronal growth cones with depleted actin veil structure.

Results

Kv3.3 triggers actin nucleation at the plasma membrane

Within the large cytoplasmic C-terminal of the Kv3.3 channel lie strings of proline residues (…PPPPPPPHPHHGS**G**GISPPPP…) conserved in mouse and humans. As will be described later, a mutation in this region (G592R) is associated with late-onset SCA13, suggesting this region plays a critical functional role. Sequence comparisons show this region is similar to regions within neural WASPs (Wiskott-Aldrich syndrome family proteins) and WAVE proteins (WASP family verprolin homologous proteins), which activate actin nucleation through Arp2/3 (Campellone and Welch, 2010). We first tested interactions of the channel with Arp2/3 by immunoblotting. Arp2/3 component Arp3 co-immunoprecipitated with wild-type Kv3.3 channels stably expressed in CHO cells (Fig. 1A, *left*). Arp3, however, was not co-immunoprecipitated in cells stably expressing the G592R mutant channel, indicating the interaction of the mutant channel with Arp2/3 is either absent or much weaker than that of the wild-type channel (Fig. 1A, *right*).

To test whether the interaction of Kv3.3 with Arp2/3 influences actin nucleation, we carried out triple channel confocal imaging of actin filaments, Arp2/3 and the Kv3.3 channel in untransfected CHO cells, and in cells transiently or stably expressing wild type Kv3.3 (Fig. 1B-E, Fig. S1A). Kv3.3 was not expressed in untransfected CHO cells (Fig. S1B); however, actin filaments were present in stress fibers within the cell body and in bundles along the cell periphery (Fig. 1B, left panels, red and green arrowheads, respectively). In untransfected

cells, Arp2/3 and actin filaments tended to colocalize in diffusely distributed puncta throughout the cell (Fig. 1B). Introduction of Kv3.3 resulted in dramatic cell rounding accompanied by colocalization of actin filaments, Arp2/3 and Kv3.3 channels to a peripheral ring-like structure near the membrane-substrate interface (Fig. 1D). Notably, stress fibers were absent or their presence severely reduced in the Kv3.3 expressing cells. Confocal Z sectioning was used to visualize the 3D distribution of actin filaments, Arp2/3 and Kv3.3 channels (cf. movies S1-S3). It was evident that all three proteins were enriched in subplasmalemmal cortical regions. Figure 1C and 1E show confocal XZ projections, i.e., cellular cross sections, of respective protein distributions for untransfected and Kv3.3 expressing cells, respectively. In cells expressing Kv3.3, actin filaments and Arp2/3 were strikingly restricted to the cell cortex relative to untransfected cells (Fig. 1C, E, F). Kv3.3 channels strongly colocalized with both actin filaments and Arp2/3 (Fig. 1E, PDM analysis indicated highest colocalization along the cortex, see Methods).

To further quantify Kv3.3 effects on cortical actin levels, we used label-free optical biosensors (the X-BODY Biosciences BIND system). This technique uses evanescent waves and resonant waveguide grating (RWG) optical biosensors to monitor changes in mass within the first ~150 nm of the membrane surface in adherent cells (Cunningham et al., 2004) (Fig.S1C). RWG optical biosensors detect changes in the index of refraction resulting from a change in mass, such as the loss of membrane-associated actin filaments, within the detection zone of the biosensor (Fleming and Kaczmarek, 2009).

We first carried out control experiments to measure changes in mass produced by activation of an endogenous G-protein-coupled receptor, or by direct activation of protein kinase C (PKC). Activation of the endogenous protease activated receptor 1 (PAR1) with the pentapeptide agonist SFLLR (10 μM), produced an increase in mass near the biosensor. Similarly, activation of PKC by 100 nM TPA (12-O-tetradecanoyl phorbol-13-acetate) produced an increase in signal, consistent with translocation of the enzyme to the plasma membrane. The amplitude of the SFLLR- and TPA-induced signal was identical in untransfected CHO cells and in those expressing Kv3.3 (Fig. 1G). In contrast, application of 10 μM latrunculin B (LatB), which sequesters actin monomers and results in actin filament depolymerization, produced a decrease in mass; moreover, the decrease was significantly greater in Kv3.3-expressing cells (Fig. 1G, $p<0.01$). These results are consistent with a greater loss of actin filaments near the plasma membrane in Kv3.3-expressing cells.

Kv3.3 inactivation is regulated by the cortical actin cytoskeleton

Patch clamp experiments were carried out in combination with a panel of pharmacological agents with well characterized effects on actin dynamics to investigate how the cortical actin filaments affect Kv3.3 ion channel gating. Under control conditions, Kv3.3 currents undergo slow and only partial inactivation, declining over hundreds of milliseconds at positive membrane potentials (Desai et al., 2008) (Fig. 2A). LatB treatment resulted in a striking progressive increase in the rate of inactivation of wild type Kv3.3 channels over tens of minutes. Because a steady state could not be reached during such recordings, we recorded Kv3.3 transfected CHO cells that were pretreated with 10 μM LatB for one hour before patch clamping. Under these conditions, the rate of inactivation was stable and very rapid,

with a time constant of 25.97 ± 2.6 msec at +70 mV leading to near complete loss of current during 600 msec depolarizations (Fig. 2A). To further quantify this effect, we measured the degree of inactivation that occurred within 100 msec of depolarization in the presence and absence of LatB (Fig. 2C). LatB did not change the voltage-dependence of activation and its effects on rate of inactivation were concentration dependent (Fig. 2B-C).

In parallel cell biological experiments, LatB treatment of Kv3.3-expressing cells was found to trigger a major loss of Arp2/3 from the cortical cytoskeleton, resulting in a 68% decrease in Arp3 cortical localization (Fig. 2G-H). A smaller (47%) change was also measured in cortical F-actin localization. LatB treatment resulted in loss of the rounded cell shape and pronounced peripheral actin ring structures typical of CHO cells expressing wild type Kv3.3 channels (Fig.S2A, top vs middle panels). The peripheral ring-like localization of Arp2/3 was also disrupted.

To further investigate the dynamic properties of the actin filaments involved in regulation of Kv3.3 channel gating, we treated cells with Cytochalasin D (CD), which mainly inhibits actin monomer addition at barbed ends, thereby inhibiting rapid actin filament polymerization. Interestingly, CD (10 μM) had no effect on the rate of inactivation of Kv3.3 channels (Fig. 2D, F) and had very little effect on cell shape (Fig.S2A) or on the localization of Arp2/3 to the cortical cytoskeleton that underlies the plasma membrane (17% decrease; Fig. 2G-H). CD also had only modest effects on cortical F-actin relative to LatB (27% vs 47% decreases for CD vs LatB, respectively). These results suggest that a relatively stable Arp2/3 dependent actin filament structure can regulate Kv3.3 channel inactivation. In support of this hypothesis, jasplakinolide, which stabilizes actin filaments, had no effect on Kv3.3 channel gating (Fig. 2E, F).

The Kv3.3-associated Arp2/3-dependent actin cytoskeleton regulates N-type inactivation

As is the case for several other potassium channels, inactivation of Kv3.3 channels occurs through an N-terminal “ball and chain” mechanism (Hoshi et al., 1990). After a channel opens, a “ball” comprised of residues at the very N-terminus of the protein interacts with residues close to the pore of the channel, occluding further ion flux (Fig. 3A).

As a test for the specificity of action of LatB, we first tested its effects on the closely-related Kv3.1 channel (Kanemasa et al., 1995). Kv3.1 lacks an N-terminal inactivation ball, and also has no WASP/WAVE-like sequence in its much shorter C-terminal domain. Kv3.1 undergoes little or no inactivation during 600 msec depolarization. LatB (10 μM) failed to produce rapid inactivation of Kv3.1 channels (Fig. 3B, F). Moreover, expression of Kv3.1 in CHO cells failed to produce any change in cell shape. The overall pattern of actin and Arp3 staining was very similar to that of untransfected cells. The cortical enrichment of actin and Arp3 in Kv3.1-expressing cells was much lower than that in Kv3.3-expressing cells and indistinguishable from that of untransfected cells (Fig. 3C,D, Fig.S1A). LatB or CD treatment of Kv3.1-expressing cells resulted in similar disruptive effects on both cortical actin structure and Arp2/3 localization (Fig.S3A-C). This is in sharp contrast with what was observed in Kv3.3-expressing cells (Fig.2H), where a CD resistant cortical actin network was present, and suggests Kv3.3 channels specifically promote generation of stable actin structures.

To further test whether the rapid inactivation produced by LatB represents an increased rate of N-terminal inactivation, we applied 10 μM LatB to Kv3.3 channels lacking the N-terminal inactivation domain (ΔN1-78 Kv3.3). In the absence of LatB, these channels display no inactivation during depolarizations lasting 600 msec, and, in the presence of LatB, inactivated only partially and very slowly (τ = 86.5 ± 6.2msec, Fig. 3E,F). This rate of inactivation was very significantly less than that of full length Kv3.3 (τ = 25.9 ± 2.8 msec).

N-type inactivation of Kv3.3 is strongly attenuated by phosphorylation of two N-terminal serine residues by PKC (Desai et al., 2008) (Fig. 3A). Consistent with this, the inactivation of wild type Kv3.3 channels treated with both LatB and the PKC activator TPA (100 nM) was slow and only partial, closely resembling that of ΔN1-78 Kv3.3 channels treated with LatB (Fig. 3E,F). In contrast, treatment of cells with both LatB and TPA in the presence of the PKC inhibitor 1 μM Bis (bisindolylmaleimide), resulted in rapid and complete channel inactivation (τ= 22.34 ± 5.7; Fig. 3E,F). Thus, at least in part, the very rapid inactivation produced by LatB in wild type Kv3.3 requires the N-terminal inactivation ball.

Inhibition of Arp2/3 or Rac signaling regulates Kv3.3 inactivation

Given the strong delocalization of cortical Arp2/3 induced by LatB (Fig. 2G-H) and coimmunoprecipitation of Arp2/3 and Kv3.3 (Fig. 1A), we tested whether Arp2/3 could be specifically involved in regulation of Kv3.3 channel gating. To this end, the specific Arp2/3 inhibitor CK666 and its inactive analog CK689 were used (Nolen et al., 2009). In voltage-clamp experiments, CK666 induced very rapid inactivation in wild type Kv3.3 channels (τ = 28.49 ± 2.3 msec), while its inactive analog CK689 had no effect (Fig. 4A, B). In addition, CK666 had a much smaller effect on ΔN1-78 Kv3.3 channels that lack the N-terminal inactivation ball (Fig. 4B). Like LatB, CK666 treatment resulted in a striking delocalization of Arp2/3 from the cell cortex of Kv3.3 expressing cells (Fig. 4E-F, 63% decrease) and a more modest decrease in cortical F-actin (Fig. 4E-F, 31% decrease). The inactive drug analog had no discernable effect on Arp2/3 localization or cortical actin structure (Fig. 4E-F, CK689; Fig.S2B). Arp2/3 inhibition resulted in disruption of peripheral lamellipodial structures, and, in some cases, cells rounded up (Fig.S2B). Finally, Arp2/3 inhibition in Kv3.1-expressing cells resulted in delocalization of the cortical Arp2/3 to a level similar to that observed after LatB or CD treatment (Fig.S3C) and relative effects on cortical actin structures were modest when compared to those observed in Kv3.3-expressing cells.

It is well known that Arp2/3 is regulated by actin nucleation promoting factors that are downstream of small GTPases Rac and/or CDC42 activity (Pollard, 2007). We found that Rac inhibition with EHT 1864 resulted in rapid inactivation of wild type Kv3.3 channels (Fig. 4C,D). In parallel cell biology experiments, Rac inhibition led to a 56% decrease in cortical Arp2/3 localization and a 44% decrease in cortical F-actin (Fig. 4G-H). Rac inhibition mimicked the effects of Arp2/3 inhibition on peripheral lamellipodial structures and cells rounding up (cf. Fig.S2B). In summary, these results suggest Arp2/3 dependent cortical actin structures that are produced by expression of Kv3.3 in the plasma membrane play a significant role in regulating the gating kinetics of these channels.

Native neuronal Kv3.3 channels are regulated by the actin cytoskeleton

Kv3.3 is highly expressed in many neurons of the auditory brainstem including the medial nucleus of the trapezoid body (MNTB) (Li et al., 2001). Co-immunostaining for Kv3.3 and the presynaptic marker syntaxin of P14 mice reveals that Kv3.3 is predominantly localized to the large presynaptic calyces of Held that synapse onto the principal neurons of this nucleus (Fig. S4A-B). No immunostaining was detected in neurons from Kv3.3$^{-/-}$ mice (data not shown). Patch clamp recordings were carried out on the calyces of P14 mice, and biotin was included in patch pipettes, allowing subsequent processing of slices to confirm that recordings had been made on presynaptic terminals (Fig. S4C-D). The rate of inactivation of voltage-dependent potassium current was accelerated within 10 minutes of treatment with 20 μM LatB in calyces from wild type animals (Fig. S4C, n = 3) but not those from Kv3.3$^{-/-}$ animals (Fig.S4D, n = 4). Moreover, an increase in inactivation in response to LatB was not detected in recordings of the somata of the postsynaptic principal neurons from either wild type or Kv3.3$^{-/-}$ mice (Figs. S4E, F, n = 3, 3), although decreases in amplitude with no change in rate of inactivation were observed in some cases (Fig. S4E). This is consistent with earlier observations that the major postsynaptic Kv3 family channel is Kv3.1 (Macica et al., 2003). These findings indicate that the linkage of Kv3.3 to the actin cytoskeleton we have characterized in transfected cells also occurs in native neurons.

G592R mutant channels are deficient in Arp2/3 interactions

A G592R mutation within the proline-rich domain in the cytoplasmic C-terminal domain of Kv3.3$\left(\ldots \mathrm{PPPPPPPHPHHGSC}\frac{\mathrm{G}}{\mathrm{R}}\mathrm{GISPPPP}\ldots\right)$ results in adult-onset SCA13 (Fig. 3A). To determine whether this mutation impairs Kv3.3 current we first expressed both mouse and human G592R Kv3.3 channels in CHO cells and characterized currents by whole cell patch clamping. Current amplitude and voltage-dependence of the mutant channels were similar to those of the wild type channels (Fig. 5A,B). Their rate of inactivation during maintained depolarization was, however, slower than that of the wild type channels. For the mouse channels, we also determined the voltage-dependence of steady-state inactivation by stepping the membrane potential from a 4 sec prepulse at potentials between −70 to +20 mV to a test potential of +20 mV for 250 ms. This was identical for the wild type and G592R channels (WT $V_{1/2}$ = 10 mV ± 0.5 mV; G592R $V_{1/2}$ =10 ± 0.3 mV).

Next we compared cytoskeletal interactions of these mutant channels with those of the wild-type channels. As described earlier, in contrast to wild-type channels, G592R Kv3.3 channels do not co-immunoprecipitate with Arp2/3 (Fig.1A). Moreover, in the label-free biosensor assay, which measures changes in mass at the plasma membrane after treatment with 10 μM LatB (see Fig. 1F), the decrease in mass near the biosensor following treatment of G592R Kv3.3 cells with LatB was not statistically different from that of untransfected cells (Fig.S1D). This contrasts sharply with wild-type Kv3.3 channels, and suggests that G592R Kv3.3 channels cannot efficiently recruit actin filaments to the plasma membrane.

To investigate this suggestion further, we compared distributions of actin filaments, Arp2/3 and channels by confocal imaging in untransfected cells or cells expressing wild type (cf. Fig.1) or G592R mutant Kv3.3 channels (Fig. 5C, D). Actin filament and Arp2/3

distributions in cells expressing G592R Kv3.3 resembled untransfected cells (compare Fig. 5C with Figs. 1B and S1A). Classical stress fibers (Fig. 5C, arrowhead) were clearly present and Arp2/3, actin filaments and mutant Kv3.3 channels were present in puncta diffusely distributed in optical sections near the substrate-membrane interface. Neither G592R Kv3.3 channels nor Arp2/3 colocalized with stress fibers (Fig. 5C, middle and bottom rows). Examination of cellular cross sections revealed a less robust patchy cortical actin structure accompanied by weaker Arp2/3 localization to the cell cortex in the mutant cells (Fig. 5D-E). Quantitative colocalization analysis by ICQ indicated that actin-Kv3.3 channel and Arp2/3- Kv3.3 channel colocalization were both significantly decreased in G592R mutants; in contrast, Arp2/3-actin filament interactions were not affected (Fig. 5F). These results suggest the G592R mutation decreases the affinity of interactions between Kv3.3 channels and Arp2/3 with little effect on Arp2/3-actin filament interactions.

Whole-cell patch clamp experiments were carried out to test the response of both mouse and human G592R Kv3.3 channels to LatB Although LatB increased inactivation of G592R Kv3.3 channels, the time constant was significantly longer than that of the wild type channels in LatB. For the mouse wild-type and G592R channels, inactivation time constants in LatB (at +70 mV) were 25.97 ± 2.6 and 72.17 ± 3.7 msec, respectively ($p = 0.0001$, $n = 4, 9$). Similarly for human wild-type and G592R channels, time constants were 31.01 ± 3.4 and 83.26 ± 8.6 msec, respectively ($p = 0.0015$, $n = 4, 4$). Moreover, in contrast to the effect of LatB on wild-type channels, inactivation of G592R channels in the presence of LatB was only partial, with only ~60% inactivation at the end of a 600 msec pulse to +70 mV (Fig. S5A). To further quantify these differences we compared the degree of inactivation that occurred within 100 msec of depolarization for the mouse and human channels in the presence and absence of LatB for both wild-type and mutant channels (Fig. S5A-C). This parameter also confirmed that the mutant channels are relatively resistant to the actions of LatB.

The slower pattern of inactivation of G592R Kv3.3 channels in the presence of LatB resembled that of wild-type channels missing the N-terminal inactivation ball (Fig. 3E), or wild-type channels exposed to a PKC activator that prevents N-type inactivation (Fig. 3E). To confirm the role of the proline-rich C-terminal domain in regulation of N-type inactivation, we tested two other C-terminal mutations, a deletion of the polyproline sequence before G592 (Δ578-588 Kv3.3), and a more extensive deletion of the cytoplasmic C-terminal domain (Δ571-769 Kv3.3) (Fig.S3C-E). Both mutants resembled wild type channels in that they inactivated only over several hundred milliseconds during depolarization. Like G592R Kv3.3, however, these two mutations inactivated more slowly and only partially after treatment with 10 μM LatB (Fig.S3C-E).

The G592R mutant channel was also relatively resistant to Arp2/3 inhibitor CK666 and the Rac inhibitor EHT 1864, compared to wild type Kv3.3 channels (Fig.S5D-G). As described earlier, CK666 (10 μM) induced rapid inactivation in wild-type channels (Fig. 4A), but the degree of inactivation within 100 msec (Fig. S5D-E) and time constant of inactivation were significantly slowed in CK666-treated G592R Kv3.3 channels (+70 mV: wild-type Kv3.3 $\tau = 28.5 \pm 2.3$ msec; G592R Kv3.3, $\tau = 62.3 \pm 13.9$ msec, $p = 0.038$). Similarly, the inactivation produced by the Rac inhibitor EHT 1864 was substantially reduced in G592R

channels, compared to wild-type Kv3.3 channels (Fig. S5F-G25 μM ETH 1864, + 70 mV, wild-type Kv3.3 τ = 18.1 ± 1.4 msec; G592R Kv3.3, τ = 46.3 ± 7.7 msec, p = 0.016, n = 4, 5).

We investigated the cell biological effects of LatB, CK666 and EHT 1864 in CHO cells expressing the G592R mutant Kv3.3 channel and compared them to effects on cells expressing wild type Kv3.3 channels (Fig. S5H for XZ view; Fig. S2C-D for XY view). In general, cortical actin networks and Arp2/3 localization were less clearly defined in the mutants (cf. Fig. 2G control vs 5D mutant) and the magnitude of the inhibitory effects on F-actin (LatB treatment), Arp2/3 (CK666 treatment) and Rac (EHT 1864 treatment) on cortical F-actin and Arp2/3 were less pronounced in the mutant-expressing cells (Fig. S5H-I). Taken together, these results suggest that a C terminal interaction site on the Kv3.3 channel potentiates cortical Arp2/3 actin filament nucleation, which in turn regulates Kv3.3 channel inactivation.

Actin veils are depleted in neuronal growth cones from G592R Kv3.3 human iPSCs

Peripheral lamellipodial domains of neuronal growth cones have two distinct actin filament structures: filopodia comprised of parallel bundles of unipolar actin filaments and branched actin filament networks referred to as “actin veils”. These structures are cross-linked into a dynamic network that undergoes retrograde actin flow which drives growth cone motility and axon guidance (Lowery and Van Vactor, 2009).

To investigate a potential role for Kv3.3 channels in regulation of growth cone actin structure, we generated induced pluripotent stem cell (iPSC) lines from a subject with the G592R mutation and differentiated these iPSCs into Kv3.3-expressing cerebral organoids in parallel with a control iPSC line (Abyzov et al., 2012; Mariani et al., 2012). Characterization of the iPSCs from the subject with the G592R mutation is shown in Figure 6. Growth cones of these cells were stained for F-actin and the Kv3.3 channel at 12 days of terminal differentiation *in vitro*. Growth cones from control stem cells exhibited filopodia and actin veil structures (Fig. 6A, red and green arrowheads, respectively) similar to that observed in vertebrate neurons in primary culture. In contrast, actin veil structure in growth cones derived from G592R Kv3.3 channel mutants was essentially absent. Filopodia, however, were still present (Fig. 6A). These findings are in line with previous studies supporting a role for Arp2/3 in generating actin veil structures (Korobova and Svitkina, 2008; Yang et al., 2012). Kv3.3 channel expression in the G592R mutant was decreased relative to controls (Fig. 6 B and C; −61.4 ± 4.6%). In addition, Kv3.3 channel interactions with actin filaments appeared to be significantly decreased (Fig. 6B and D; −45.1 ± 4.2%). These findings support the hypothesis that Kv3.3 channels regulate Arp2/3 dependent actin nucleation in growth cones of neurons expressing Kv3.3. This process appears to be severely compromised in a G592R mutant that results in spinocerebellar ataxia.

Kv3.3 actions on the cortical cytoskeleton are mediated by Hax-1

The effects of Kv3.3 channels could be mediated by a direct interaction of the channel with Arp2/3 to stimulate actin nucleation or by its interaction with known regulators of this complex. Some channels interact with the WAVE regulatory complex (WRC) through a

consensus WRC interacting receptor sequence (WIRS) (Chen et al., 2014; Chia et al., 2014). This interaction allows membrane proteins to recruit the WAVE regulatory complex to the membrane; Kv3.3 does not, however, contain a WIRS-like sequence. To identify potential Kv3.3 interacting proteins, we carried out a high-stringency yeast-two hybrid screen of a normalized human brain cDNA library using the full C-terminal Kv3.3 domain as bait. The anti-apoptotic protein Hax-1(Chao et al., 2008; Fadeel and Grzybowska, 2009) was the dominant Kv3.3-interacting protein, found in nine independent sequenced positive clones (Fig. 7A). We confirmed Hax-1 interaction with both wild type and G592R Kv3.3 channels by co-immunoprecipitation from membrane fractions from cells stably expressing these channels (Fig. 7B, *middle* and *right* panels, respectively). In addition, native neuronal Kv3.3 from mouse brain co-immunoprecipitated with Hax-1 (Fig.7 B, *left* panel). In parallel cell biology experiments, Hax-1 was cortically enriched in cells expressing wild type Kv3.3 channels; while expression of mutant channels abolished Hax-1 cortical enrichment (Fig.S6A-C).

To investigate a potential role for Hax-1 in the effects of wild type Kv3.3 channels on the actin cytoskeleton, we suppressed Hax-1 expression using a heterogeneous mixture of siRNAs (endoribonuclease-prepared siRNAs). We were able to reduce Hax-1 protein levels in wild type Kv3.3 cells to ~25% of that in control Kv3.3 cells, or cells treated with scrambled siRNAs, without loss of cell viability (Fig. S7A-B). Immunocytochemistry analysis indicated that cortical Hax-1 localization in Hax-1 siRNA cells was reduced to ~25% of that in scrambled siRNA cells (Fig.S7C-E). Cell morphology as well as actin filament and Arp2/3 distributions closely resembled those observed in untransfected cells or those expressing G592R Kv3.3 mutant channels. Cells became generally flatter, with the reappearance of actin stress fibers (Fig. 7C). Hax-1 siRNA treatment resulted in loss of actin and Arp3 from the cell cortex and quantitative redistribution to the cytoplasm (Fig. 7D,E).

In voltage-clamp recordings of wild type Kv3.3 channel currents in Hax-1 siRNA cells, redistribution of actin and Arp3 from the cortex to the cytoplasm was correlated with a significant increase in the rate of inactivation (Fig. 7F). The degree of inactivation within 100 msec of the peak current at +70 mV (I_{100}/I_{peak}) was 0.05 ± .01 in cells treated with scrambled siRNA (n = 6) and increased to 0.21 ± .02 in Hax-1 depleted cells (n = 5, $p < 0.0002$). The time constant of inactivation also decreased from 342 ± 37 msec to 234 ± 15 msec on decreasing Hax-1 levels ($p < 0.05$).

Previous work has shown that Hax-1 can act as a scaffold for Rac and cortactin (Gomathinayagam et al., 2014), each of which in turn could activate Arp2/3. To test whether Hax-1 coordinates Rac and cortactin, we first compared Rac distribution in cells expressing wild type Kv3.3 channels and those with the G592R mutation. Rac was highly localized to the cell cortex in wild type Kv3.3 cells and delocalized in mutant cells (Fig.S6D-F). Next, we examined the behavior of WAVE3, an Arp2/3 nucleation promoting factor activated by Rac. We found that both wild type and G592R Kv3.3 channels were co-immunoprecipitated by WAVE3 (Fig S7I). As with actin and Arp3, Hax-1 siRNA treatment resulted in WAVE3 delocalization from the cell cortex and quantitative redistribution to the cytoplasm (Fig. S7F-H).

Finally, we investigated a role for cortactin. Cortactin co-immunoprecipitated with wild type Kv3.3, and was localized to the cortical cytoskeleton in Kv3.3-expresing cells (Fig. 7G, H; Fig. S6G for XY view); however, little or no cortactin co-immunoprecipitated with the mutant G592R Kv3.3 channel (Fig. 7G, right). Cortical localization of cortactin in G592R mutant cells was also greatly compromised (Fig.7H,I; Fig. S6G for XY view).

Discussion

Using multiple aproaches we found that the Kv3.3 potassium channel regulates Arp2/3 dependent cortical actin nucleation mediated by Hax-1. The resulting cortical actin structures interact with the channel's gating machinery to slow its inactivation rate during sustained membrane depolarizations. Moreover, a mutation that leads to late-onset spinocerebellar ataxia type 13 results in destabilization of channel dependent cortical actin structures, with resultant changes in channel gating and neuronal growth cone morphology.

Many ion channels interact with the actin cytoskeleton. As one example, α-actinin mediates interactions of L-type calcium channels with actin filaments required for channel retention in the plasma membrane (Zhao et al., 2013). Properties of the acid-sensing ASIC1a channel are modified by α-actinin interactions (Schnizler et al., 2009). Many other channel-actin filament interactions are likely mediated by the WIRS sequence motif, which facilities membrane protein linkage to the WAVE complex (Chen et al., 2014; Chia et al., 2014). The present findings are, to our knowledge, the first evidence of an ion channel exerting regulatory effects on Arp2/3 dependent actin cytoskeleton.

During development, voltage-dependent potassium channels with characteristics of the Kv3-family are found at high levels in neuronal growth cones (Huang et al., 2012; Pollock et al., 2005). Thus, in neurons expressing Kv3.3, actin filament dynamics are likely to be affected by the presence of this channel. In support of this idea, actin veils were essentially absent in neuronal growth cones derived from human induced pluripotent stem cells (iPSCs) bearing the G592R Kv3.3 mutation. Failure of the mutant channels to engage appropriately with the cytoskeleton may therefore contribute to the resultant spinocerebellar ataxia.

Our results also suggest that the Kv3.3-induced Arp2/3 dependent structures are remarkably stable. The classical picture of Arp2/3 function involves nucleation of daughter filaments at actin network branch points followed by barbed end elongation until their ends are capped (Pollard, 2007). Significantly, we found that cytochalasin D, which would inhibit barbed end assembly (MacLean-Fletcher and Pollard, 1980), had no effect on Kv3.3 channel inactivation (Fig. 2D and F) and remarkably little effect on cortical actin structure (Fig. 2G-H). These findings strongly suggest that juxta-membrane barbed ends in these structures are *already* capped which would contribute to their stability. Our parallel finding that actin filament stabilization by jasplakinolide had no effect on Kv3.3 channel gating kinetics reinforces the hypothesis that these Arp2/3 dependent structures are very stable.

What molecular processes could be involved in generation of these stable cortical actin structures? Our data indicate that Hax-1 interacts with the C-terminal domain of Kv3.3 and becomes enriched at the cell cortex. Hax-1 has been identified as an anti-apoptotic protein

required for the survival of cerebellar neurons (Chao et al., 2008) that also interacts with cortactin and Rac (Gomathinayagam et al., 2014; Suzuki et al., 1997). We found that cortactin associates with Kv3.3 and is localized to the cell cortex along with Hax-1. Cortactin is an SH3 domain containing type II actin nucleation promoting factor (NPF) that can also stabilize Arp2/3 dependent actin filament branches (Weaver et al., 2001). We found that the G592R mutant binds cortactin less effectively than the wild type channel, delocalizes cortactin from the cell cortex, and is less efficient in generating Arp2/3-dependent actin structures (Fig. 7). Although we cannot rule out an Arp2/3 NPF role for channel-associated cortactin, the strong effects of Rac inhibition (Fig. 4) suggest that Rac activation of WAVE is primarily responsible for building channel dependent Arp2/3 actin networks. Taken together, the above results are consistent with Hax-1 coordinating assembly of Arp2/3 dependent actin networks by Rac/WAVE3 activation and subsequent stabilization by cortactin.

Our evidence indicates that Kv3.3-dependent cortical actin structures regulate the channel's gating behavior. Inhibition of Arp2/3 or Rac, or down-regulation of Hax-1, all increased channel inactivation rates. Although decreasing Hax-1 levels had less marked effects than pharmacological Arp2/3 or Rac inhibition, this is likely due to the limitations of siRNA as Hax-1 levels could only be reduced by ~75% without affecting cell viability. Several findings also demonstrate that N-type inactivation, i.e. the ability of the N-terminal inactivation ball to block the Kv3.3 channel, is primarily accelerated by these treatments. Specifically, the effects of cytoskeletal disruption were greatly attenuated in the closely related Kv3.1 channel, which lacks an N-terminal inactivation ball, and also in Kv3.3 channels lacking the N-terminal inactivation ball or phosphorylated by PKC, which prevents N-type inactivation. The simplest interpretation is that Arp2/3 itself, or capped actin filaments nucleated off the complex, normally impedes access of the N-terminal inactivation ball to the channel pore. Accordingly, actin filament disassembly or loss of Arp2/3 would allow the N-terminus to block the pore more rapidly following channel activation. We note that in N-terminal or C-terminal mutations, LatB treatment or Arp2/3 or Rac inhibition resulted in much slower and only partial inactivation. Although the nature of this slower inactivation was not tested, it may represent an enhancement of "C-type inactivation" , a constriction of the pore during sustained depolarization (Hoshi and Armstrong, 2013).

The interaction between Kv3.3 and Hax-1 provides potential links between SCA13 mutations and degeneration of neurons such as cerebellar Purkinje cells. Although Hax-1 binds G592R Kv3.3, its ability to trigger Arp2/3 dependent actin nucleation and to link N-type inactivation to the cytoskeleton is impaired when bound to this mutant channel. Thus, other actions of Hax-1, such as suppression of caspase activation and apoptosis signaling may also be impaired (Fadeel and Grzybowska, 2009; Simmen, 2011). Moreover, effects of cortical Kv3.3-Hax-1 interactions are likely to be abolished in disease-causing mutations that prevent trafficking of Kv3.3 to the plasma membrane (Gallego-Iradi et al., 2014). It remains to be determined how other SCA13 mutations that, like G592R Kv3.3, result in channels with altered gating behavior alter the pro-survival actions of Hax-1 within cells.

Experimental procedures

General methods

Standard methods were used for maintaining and transfecting CHO cells, as well as membrane isolation, Western blotting , site-directed mutagenesis and immunocytochemistry. These techniques and the methods described briefly below, are described in detail in Extended Experimental Procedures.

Resonance wavelength grating optical biosensor assays

Cells were plated on poly-l-lysine/laminin coated TiO_2 384-well BIND biosensor plates, which were then transferred to an X-BODY Biosciences BIND Scanner for analysis (Fleming and Kaczmarek, 2009).

Confocal microscopy

Fluorescent images were acquired using a spinning disk confocal system (Revolution XD; Andor) with a CSU-X1 confocal head (Yokogawa) mounted on an inverted microscope (TE 2000E; Nikon) with Perfect Focus, using an EMCCD camera (iXonEM +888; Andor). Transillumination was provided by a halogen lamp and controlled by a SmartShutter (Sutter Instrument). Confocal excitation was provided by an Andor laser combiner with three laser lines at 488, 561, and 647 nm. Emission wavelength was controlled using a filter wheel (LB10W-2800; Sutter Instrument) outfitted with bandpass filters from Chroma Technology Corp. A Nikon CFI Plan Apo 100x, 1.4 NA objective was used. Image acquisition and all other peripherals were controlled by Micro-Manager open source microscopy software (Edelstein et al., 2014).

Image processing

Image processing was performed in Image J open source software (NIH: http://imagej.nih.gov/ij/index.html). Fluorescent images were background subtracted prior to quantitative analysis. For display only, images were convolved with a Gaussian kernel, followed by an unsharp mask and scaled according to a linear look up table. A binary mask was used to eliminate noise outside the cell. The lone exception is the stem cell data in Figure 6. See Supplemental Experimental Procedures for details re quantitative image analysis.

Electrophysiology

Patch Clamp Recordings from CHO cells and from MNTB neurons in brain slices (13-17 day old BL6 wild type and $Kv3.3^{-/-}$ mice) were carried out as described previously (Desai et al., 2008; Yang and Wang, 2006). All procedures described followed National Institutes of Health guidelines outlined in “Preparation and Maintenance of Higher Animals During Neuroscience Experiments” (publication 91-3207). Procedures were approved by the Institutional Animal Care and Use Committee at the Yale University School of Medicine.

Production of iPSC lines

We produced 3 lines by transducing primary fibroblast culture derived from a skin biopsy of a patient with G592R mutation with four canonical Yamanaka factors as described (Takahashi et al., 2007).

Supplementary Material

Refer to Web version on PubMed Central for supplementary material.

Acknowledgements

This work was supported by NIH grants DC01919 (to LKK) and NS028695 (to PF) and the Harris Professorship fund (to FMV). We also very gratefully acknowledge the support of Lisa and Mark Shufro.

References

Abyzov A, Mariani J, Palejev D, Zhang Y, Haney MS, Tomasini L, Ferrandino AF, Rosenberg Belmaker LA, Szekely A, Wilson M, et al. Somatic copy number mosaicism in human skin revealed by induced pluripotent stem cells. Nature. 2012; 492:438–442. [PubMed: 23160490]

Campellone KG, Welch MD. A nucleator arms race: cellular control of actin assembly. Nat Rev Mol Cell Biol. 2010; 11:237–251. [PubMed: 20237478]

Chang SY, Zagha E, Kwon ES, Ozaita A, Bobik M, Martone ME, Ellisman MH, Heintz N, Rudy B. Distribution of Kv3.3 potassium channel subunits in distinct neuronal populations of mouse brain. The Journal of Comparative Neurology. 2007; 502:953–972. [PubMed: 17444489]

Chao JR, Parganas E, Boyd K, Hong CY, Opferman JT, Ihle JN. Hax1-mediated processing of HtrA2 by Parl allows survival of lymphocytes and neurons. Nature. 2008; 452:98–102. [PubMed: 18288109]

Chen B, Brinkmann K, Chen Z, Pak CW, Liao Y, Shi S, Henry L, Grishin NV, Bogdan S, Rosen MK. The WAVE regulatory complex links diverse receptors to the actin cytoskeleton. Cell. 2014; 156:195–207. [PubMed: 24439376]

Chia PH, Chen B, Li P, Rosen MK, Shen K. Local F-actin network links synapse formation and axon branching. Cell. 2014; 156:208–220. [PubMed: 24439377]

Cunningham BT, Li P, Schulz S, Lin B, Baird C, Gerstenmaier J, Genick C, Wang F, Fine E, Laing L. Label-Free Assays on the BIND System. Journal of Biomolecular Screening. 2004; 9:481–490. [PubMed: 15452334]

Desai R, Kronengold J, Mei J, Forman SA, Kaczmarek LK. Protein Kinase C Modulates Inactivation of Kv3.3 Channels. Journal of Biological Chemistry. 2008; 283:22283–22294. [PubMed: 18539595]

Edelstein AD, Tsuchida MA, Amodaj N, Pinkard H, Vale RD, Stuurman N. Advanced methods of microscope control using muManager software. J Biol Methods. 2014:1.

Fadeel B, Grzybowska E. HAX-1: a multifunctional protein with emerging roles in human disease. Biochim Biophys Acta. 2009; 1790:1139–1148. [PubMed: 19524642]

Fleming MR, Kaczmarek LK. Use of optical biosensors to detect modulation of Slack potassium channels by G protein-coupled receptors. Journal of Receptors and Signal Transduction. 2009; 29:173–181. [PubMed: 19640220]

Gallego-Iradi C, Bickford JS, Khare S, Hall A, Nick JA, Salmasinia D, Wawrowsky K, Bannykh S, Huynh DP, Rincon-Limas DE, et al. KCNC3(R420H), a K(+) channel mutation causative in spinocerebellar ataxia 13 displays aberrant intracellular trafficking. Neurobiology of disease. 2014; 71:270–279. [PubMed: 25152487]

Gomathinayagam R, Muralidharan J, Ha JH, Varadarajalu L, Dhanasekaran DN. Hax-1 is required for Rac1-Cortactin interaction and ovarian carcinoma cell migration. Genes Cancer. 2014; 5:84–99. [PubMed: 25053987]

Hoshi T, Armstrong CM. C-type inactivation of voltage-gated K+ channels: pore constriction or dilation? J Gen Physiol. 2013; 141:151–160. [PubMed: 23319730]

Hoshi T, Zagotta W, Aldrich R. Biophysical and molecular mechanisms of Shaker potassium channel inactivation. Science. 1990; 250:533–538. [PubMed: 2122519]

Huang C-Y, Chu D, Hwang W-C, Tsaur M-L. Coexpression of high-voltage-activated ion channels Kv3.4 and Cav1.2 in pioneer axons during pathfinding in the developing rat forebrain. The Journal of Comparative Neurology. 2012; 520:3650–3672. [PubMed: 22473424]

Irie T, Matsuzaki Y, Sekino Y, Hirai H. Kv3.3 channels harbouring a mutation of spinocerebellar ataxia type 13 alter excitability and induce cell death in cultured cerebellar Purkinje cells. The Journal of Physiology. 2014; 592:229–247. [PubMed: 24218544]

Kanemasa T, Gan L, Perney TM, Wang LY, Kaczmarek LK. Electrophysiological and pharmacological characterization of a mammalian Shaw channel expressed in NIH 3T3 fibroblasts. J Neurophysiol. 1995; 74:207–217. [PubMed: 7472324]

Korobova F, Svitkina T. Arp2/3 complex is important for filopodia formation, growth cone motility, and neuritogenesis in neuronal cells. Mol Biol Cell. 2008; 19:1561–1574. [PubMed: 18256280]

Lee A, Fakler B, Kaczmarek LK, Isom LL. More than a pore: ion channel signaling complexes. J Neurosci. 2014; 34:15159–15169. [PubMed: 25392484]

Li W, Kaczmarek LK, Perney TM. Localization of two high-threshold potassium channel subunits in the rat central auditory system. J Comp Neurol. 2001; 437:196–218. [PubMed: 11494252]

Lowery LA, Van Vactor D. The trip of the tip: understanding the growth cone machinery. Nat Rev Mol Cell Biol. 2009; 10:332–343. [PubMed: 19373241]

Macica CM, von Hehn CA, Wang LY, Ho CS, Yokoyama S, Joho RH, Kaczmarek LK. Modulation of the kv3.1b potassium channel isoform adjusts the fidelity of the firing pattern of auditory neurons. J Neurosci. 2003; 23:1133–1141. [PubMed: 12598601]

MacLean-Fletcher S, Pollard TD. Mechanism of action of cytochalasin B on actin. Cell. 1980; 20:329–341. [PubMed: 6893016]

Mariani J, Simonini MV, Palejev D, Tomasini L, Coppola G, Szekely AM, Horvath TL, Vaccarino FM. Modeling human cortical development in vitro using induced pluripotent stem cells. Proc Natl Acad Sci U S A. 2012; 109:12770–12775. [PubMed: 22761314]

Middlebrooks JC, Nick HS, Subramony SH, Advincula J, Rosales RL, Lee LV, Ashizawa T, Waters MF. Mutation in the Kv3.3 Voltage-Gated Potassium Channel Causing Spinocerebellar Ataxia 13 Disrupts Sound-Localization Mechanisms. PLoS ONE. 2013; 8:e76749. [PubMed: 24116147]

Minassian NA, Lin M-CA, Papazian DM. Altered Kv3.3 channel gating in early-onset spinocerebellar ataxia type 13. The Journal of Physiology. 2012; 590:1599–1614. [PubMed: 22289912]

Nolen BJ, Tomasevic N, Russell A, Pierce DW, Jia Z, McCormick CD, Hartman J, Sakowicz R, Pollard TD. Characterization of two classes of small molecule inhibitors of Arp2/3 complex. Nature. 2009; 460:1031–1034. [PubMed: 19648907]

Pollard TD. Regulation of actin filament assembly by Arp2/3 complex and formins. Annual review of biophysics and biomolecular structure. 2007; 36:451–477.

Pollock NS, Atkinson-Leadbeater K, Johnston J, Larouche M, Wildering WC, McFarlane S. Voltage-gated potassium channels regulate the response of retinal growth cones to axon extension and guidance cues. The European journal of neuroscience. 2005; 22:569–578. [PubMed: 16101738]

Rudy B, McBain C. Kv3 channels: Voltage-gated K+ channels designed for high-frequency repetitive firing. Trends Neurosci. 2001; 24:517–526. [PubMed: 11506885]

Sacco T, De Luca A, Tempia F. Properties and expression of Kv3 channels in cerebellar Purkinje cells. Molecular and Cellular Neuroscience. 2006; 33:170–179. [PubMed: 16949837]

Schnizler MK, Schnizler K, Zha XM, Hall DD, Wemmie JA, Hell JW, Welsh MJ. The cytoskeletal protein alpha-actinin regulates acid-sensing ion channel 1a through a C-terminal interaction. J Biol Chem. 2009; 284:2697–2705. [PubMed: 19028690]

Simmen T. Hax-1: a regulator of calcium signaling and apoptosis progression with multiple roles in human disease. Expert opinion on therapeutic targets. 2011; 15:741–751. [PubMed: 21391832]

Suzuki Y, Demoliere C, Kitamura D, Takeshita H, Deuschle U, Watanabe T. HAX-1, a novel intracellular protein, localized on mitochondria, directly associates with HS1, a substrate of Src family tyrosine kinases. The Journal of Immunology. 1997; 158:2736–2744. [PubMed: 9058808]

Takahashi K, Tanabe K, Ohnuki M, Narita M, Ichisaka T, Tomoda K, Yamanaka S. Induction of pluripotent stem cells from adult human fibroblasts by defined factors. Cell. 2007; 131:861–872. [PubMed: 18035408]

Waters M, Minassian N, Stevanin G, Figueroa K, Bannister J, Nolte D, Mock A, Evidente V, Fee D, Muller U, et al. Mutations in the voltage-gated potassium channel KCNC3 cause degenerative and developmental CNS phenotypes. Nat Genet. 2006; 38:447–451. [PubMed: 16501573]

Weaver AM, Karginov AV, Kinley AW, Weed SA, Li Y, Parsons JT, Cooper JA. Cortactin promotes and stabilizes Arp2/3-induced actin filament network formation. Curr Biol. 2001; 11:370–374. [PubMed: 11267876]

Yang Q, Zhang XF, Pollard TD, Forscher P. Arp2/3 complex-dependent actin networks constrain myosin II function in driving retrograde actin flow. J Cell Biol. 2012; 197:939–956. [PubMed: 22711700]

Yang YM, Wang LY. Amplitude and kinetics of action potential-evoked Ca2+ current and its efficacy in triggering transmitter release at the developing calyx of held synapse. J Neurosci. 2006; 26:5698–5708. [PubMed: 16723526]

Zhang Y, Kaczmarek LK. Kv3.3potassium channels and spinocerebellar ataxia. J Physiol. 2015 in press.

Zhao J, Bruck S, Cemerski S, Zhang L, Butler B, Dani A, Cooper JA, Shaw AS. CD2AP links cortactin and capping protein at the cell periphery to facilitate formation of lamellipodia. Mol Cell Biol. 2013; 33:38–47. [PubMed: 23090967]

Highlights

- Kv3.3 ion channels coordinate assembly of Arp2/3 dependent cortical actin networks
- These actin networks slow the rate of Kv3.3 channel closing during depolarization
- Network assembly is coordinated by Hax-1, a Rac and cortactin binding protein
- Cerebellar ataxia is correlated with a channel mutation that blocks network assembly

Kv3.3 channels coordinate assembly of cortical Arp2/3-dependent actin networks that in turn interact with channels to slow their rate of closing during sustained depolarization, suggesting a basis for how known channel mutations result in abnormal neuronal growth during development and cause cerebellar ataxia in human patients.

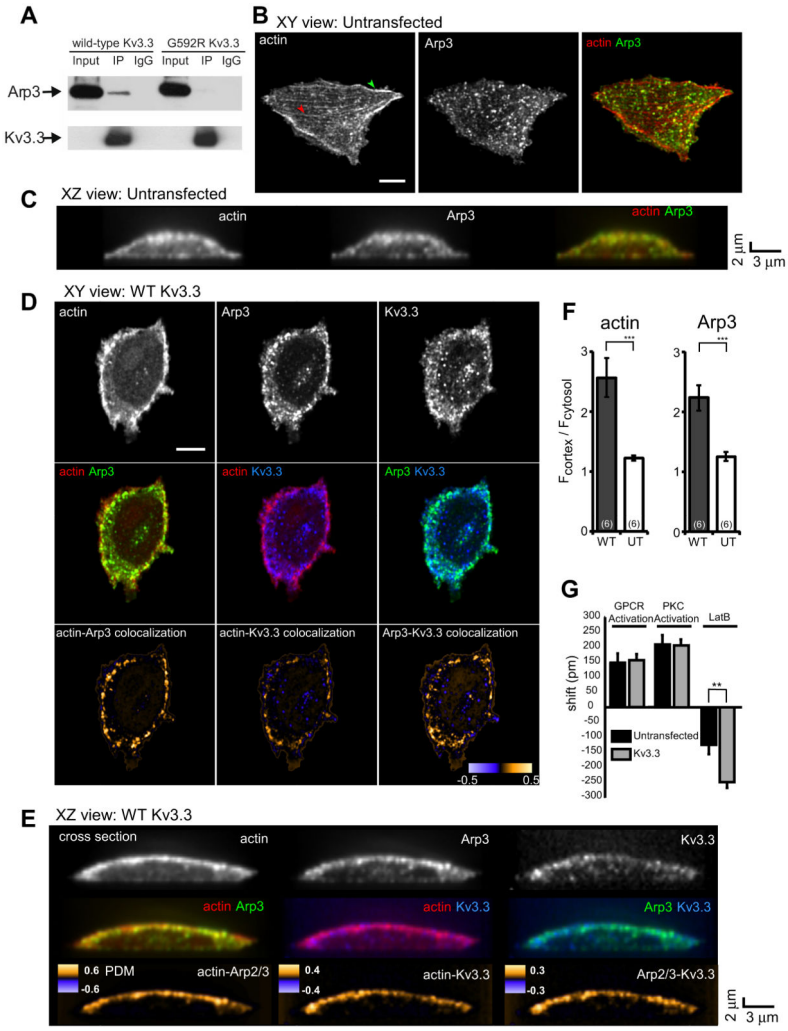

Figure 1. Kv3.3 triggers Arp2/3 dependent cortical actin filament assembly

(A) Western blots for Arp3 and Kv3.3 demonstrating Arp2/3 is co-immunoprecipitated with wild-type Kv3.3 channels (left) but not G592R Kv3.3 (right).

(B-C) Fluorescent labeling of untransfected CHO cells with Alexa 594 phalloidin and Arp3 antibody after fixation. *B*: XY view of actin (left), Arp3 (middle) or overlay of actin and Arp3 (right) images; red and green arrowheads: stress fibers and peripheral actin bundles, respectively; *C*: XZ view of actin (left), Arp3 (middle) or overlay of actin and Arp3 (right) images.

(D-E) CHO cells transfected with wild type Kv3.3 labeled with Alexa 594 phalloidin, Arp3 antibody and Kv3.3 antibody after fixation. XY view (*D*) and XZ view (*E*): top panel: actin (left), Arp3 (middle) or Kv3.3 (right); middle row: overlay of actin and Arp3 (left), actin and Kv3.3 (middle) or Arp3 and Kv3.3 (right); bottom row: PDM (product of the differences from the mean) image assessing colocalization levels between actin and Arp3 (left), actin and Kv3.3 (middle) or Arp3 and Kv3.3 (right); scale bar: 5 µm.

(F) Quantification of cortical enrichment in CHO cells transfected with wild type or untransfected cells: actin (*left*), Arp2/3 (*right*); n = 6 cells per condition, 3 measurements per cell; Data provided as mean +/− SEM; *** $p < 0.001$, two-tailed unpaired t test.

(G) Mass liberated by LatB at the surface of Kv3.3 expressing cells is greater than untransfected cells. Mass measured by changes in peak refraction wavelength, in response to the pentapeptide SFLLR (10 μM), TPA (100 nM) or LatB (10 μM). Values are mean ± SEM, n = 9, ** p <0.01 using t test.

See also Figure S1 and Movies 1-3.

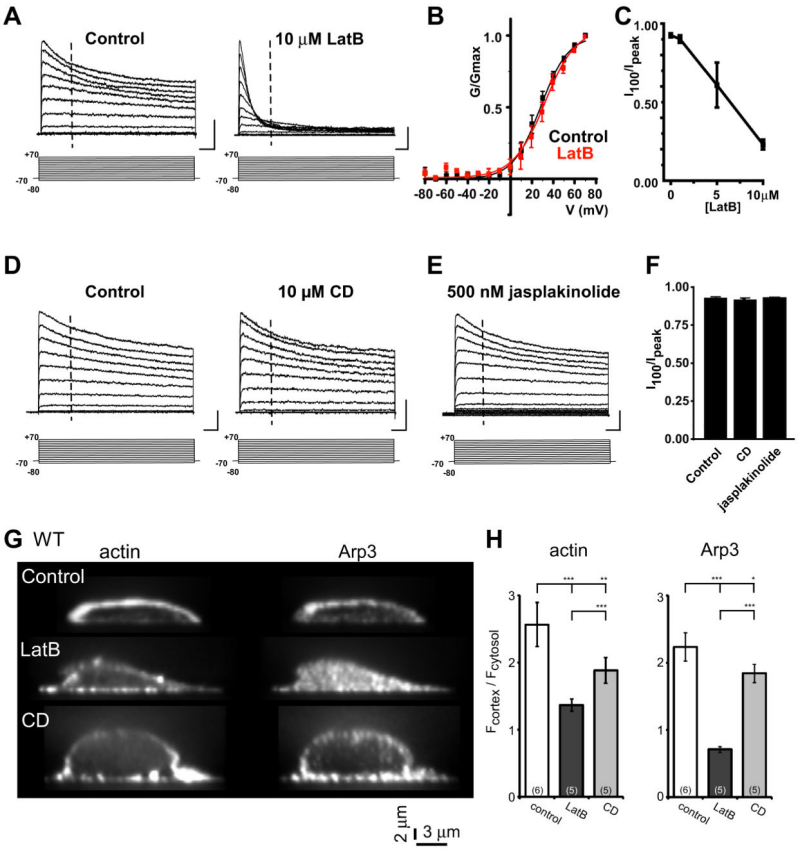

Figure 2. Wild type Kv3.3 inactivation is greatly increased by sequestration of monomeric actin

(A) Representative Kv3.3 currents in CHO cells evoked by commands to potentials between −80 and +70 mV before (*left*) and after (*right*) incubation with LatB 10 μM for 1 hour. Dashed vertical lines 100 msec after depolarization.

(B) Normalized G/Gmax curves for Kv3.3 currents in the presence and absence of LatB (10 μM). Mean ± SEM, n = 9.

(C) Dose-response for LatB effects on channel inactivation within 100 msec of the peak current (I_{100}/I_{peak}) (n = 5 each concentration).

(D) Control Kv3.3 currents (*left*) or currents after cytochalasin D (10 μM) for 1 hour (*right*).

(E) Kv3.3 currents in jasplakinolide (500 nM). Scale bars: *A*, *D*, *E*, 1 nA, 50 msec.

(F) Channel inactivation ± SEM within 100 msec of peak current at +70 mV (I_{100}/I_{peak}) for Kv3.3 channels in the absence (Control, n = 7) or presence of cytochalasin D (10 μM, n = 4) or jasplakinolide (500 nM, n = 7).

(G) CHO expressing Kv3.3 channels and labeled with Alexa 594 phalloidin and Arp3 antibody after fixation. Cross section (XZ view) of actin (left) and Arp3 (right) images; Top: control (0.1% DMSO, 1hr); Middle: Latrunculin B (LatB, 10 μM, 1hr); Bottom: Cytochalasin D (CD, 10 μM, 1hr).

(H) Quantification of cortical enrichment expressed as ratio of the mean fluorescent intensity in cortex relative to cytosol in CHO cells expressing wild type Kv3.3 channels. Actin (left) and Arp2/3 (right) cortical levels assessed under: control, LatB treatment (10 μM, 1hr), or Cytochalasin D treatment (10 μM, 1hr); Parentheses indicate number of cells measured, 3

measurements per cell; Values are mean ± SEM, * $p < 0.05$; ** $p < 0.01$; *** $p < 0.001$, two-tailed unpaired t test.
See also Figures S2 and S4.

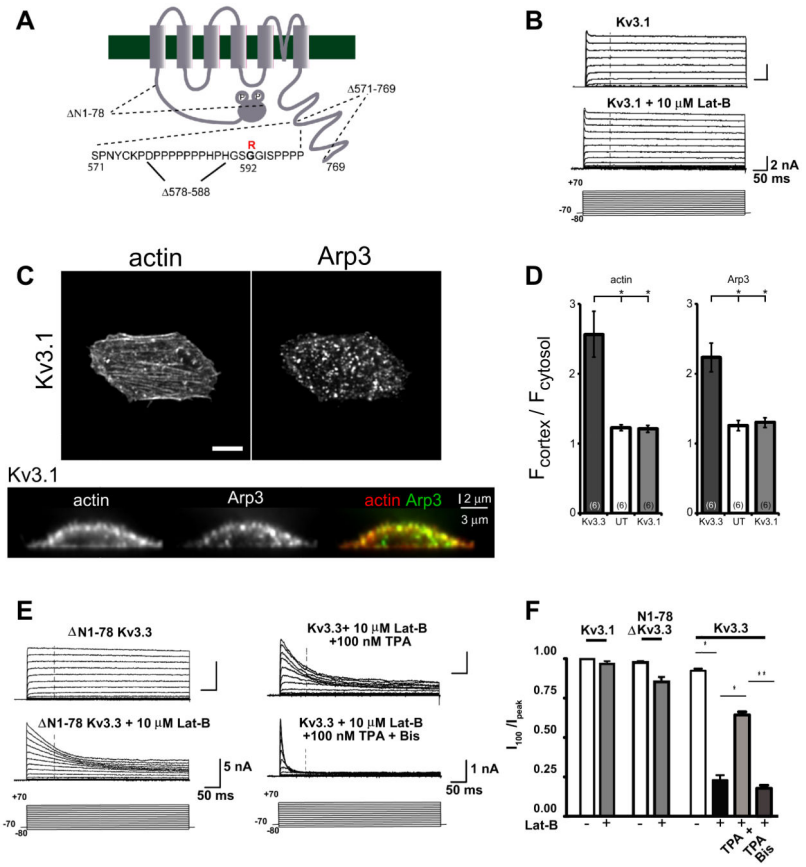

Figure 3. Cytoskeletal agents regulate N-type inactivation

(A) Kv3.3 channel schematic indicating deletions and mutation loci.

(B) Representative currents from CHO cells expressing related channel Kv3.1, in the absence and presence of 10 μM LatB. Dashed vertical lines 100 msec after onset of depolarization.

(C) Labeling of Kv3.1 expressing CHO cells with Alexa 594 phalloidin and Arp3 antibody after fixation. Top panel: XY view of actin (left) and Arp3 (right), scale bar: 5 μm; Bottom: XZ view of actin (left), Arp3 (middle) or overlay of actin and Arp3 (right).

(D) Quantification of cortical enrichment (as in Fig. 2H) in CHO cells transfected with wild type Kv3.3 or Kv3.1 or untransfected CHO cells (UT): actin (*left*), Arp2/3 (*right*); n = 6 cells per condition, 3 measurements per cell; Values are mean ± SEM. For comparisons between Kv3.3, Kv3.1 and untranfected CHO cells, $p < 1 \times 10^{-11}$ with single factor ANOVA, asterisk indicates significant difference using Tukey's HSD post hoc analysis.

(E) Left: Currents recorded from cells expressing channels with N-terminal truncation ΔN1-78 Kv3.3 in the absence and presence of 10 μM LatB. Right: Currents recorded from cells expressing mouse Kv3.3 after incubation with both the PKC activator TPA (100 nM) and LatB (10 μM) for 1hour (*top traces*), and currents under the same conditions in the presence of the PKC inhibitor Bis (1 μM) (*bottom traces*).

(F) Bar graphs showing degree of inactivation ± SEM within 100 msec of the peak current at +70 mV (I_{100}/I_{peak}) for each of the conditions in panels B and E (Kv3.1, n = 4, 4; ΔN1-78

Kv3.3, n = 6, 6; Kv3.3 + TPA + LatB, n = 4; Kv3.3 + TPA + LatB + Bis, n = 4, * $p < 0.05$, ** $p < 0.01$, two-tailed unpaired t test). See also Figure S3.

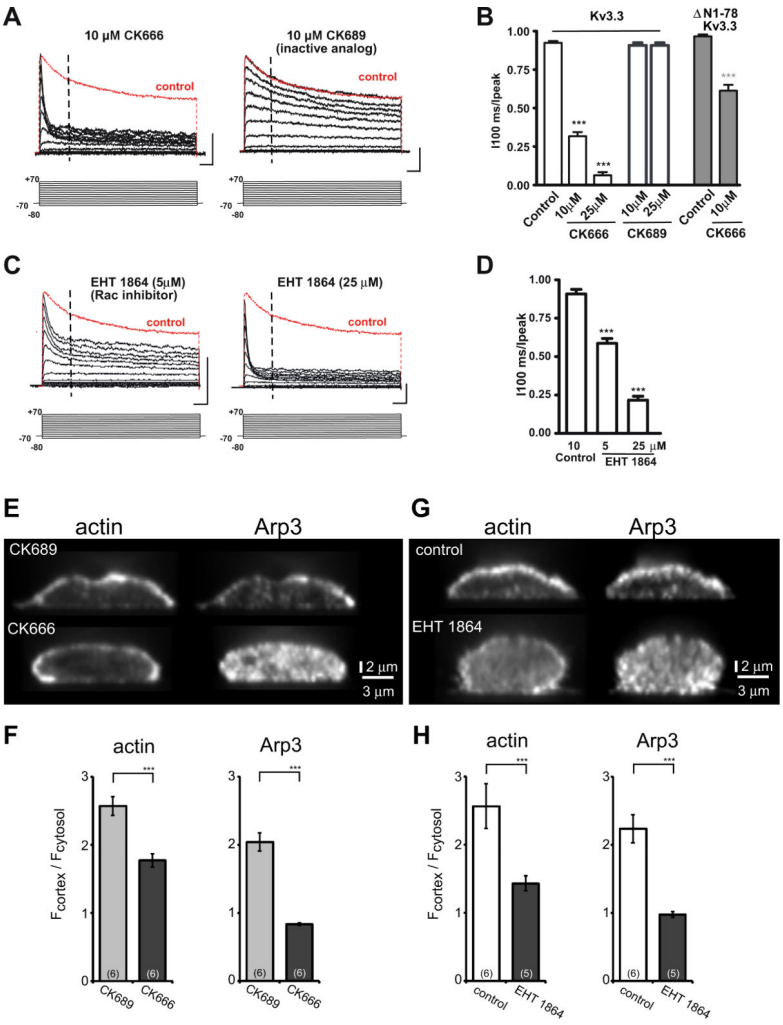

Figure 4. Inhibition of Arp2/3 or Rac increases Kv3.3 inactivation

(A) Representative voltage-clamp mouse Kv3.3 currents after incubation with Arp2/3 inhibitor CK666 (10 μM) for 30 min (*left panel*) or inactive analog CK689 (*right panel*). Representative control currents at +70 mV (red). Dashed vertical lines at 100 msec after depolarization.

(B) Degree of inactivation within 100 msec of the peak current at +70 mV (I_{100}/I_{peak}) for wild type Kv3.3 expressing cells in the absence (Control) or presence of 10 or 25 μM CK666 or CK689 or for N-terminal truncation ΔN1-78 Kv3.3 expressing cells in the absence and presence of 10 μM CK666. Values are mean ± SEM, n = 4, *** $p < 0.001$, two-tailed unpaired t test.

(C) Currents recorded after incubation with 5 or 25 μM Rac inhibitor EHT 1864 for 1 hour.

(D) Degree of inactivation within 100 msec of peak current at +70 mV (I_{100}/I_{peak}) in the absence and presence of EHT 1864. Values are mean ± SEM, n = 4, 4 for 5 and 25 mM EHT 1864, respectively. *** $p < 0.001$ two-tailed unpaired t test. Scale bars *A* and *C*, 1 nA, 50 msec.

(E) CHO cells transfected with wild type Kv3.3 labeled with Alexa 594 phalloidin and Arp3 antibody after fixation. Cross section (XZ view) of actin (left) and Arp3 (right); Top row: CK689 (50 μM, 1hr); bottom row: CK666 (50 μM, 1hr);
(F) Quantification cortical enrichment levels in CHO cells transfected with wild type Kv3.3 channels: actin (left) and Arp2/3 (right) after CK689 treatment (50 μM, 1hr) or CK666 treatment (50 μM, 1hr); Parentheses: number cells measured, 3 measurements per cell; Values are mean ± SEM, *** $p < 0.001$ two-tailed unpaired t test.
(G) Cells transfected with wild type Kv3.3 labeled with Alexa 594 phalloidin and Arp3 antibody after fixation. Cross section (XZ view) of actin (left) and Arp3 (right) images; Top row: control (0.1% DMSO, 1hr); Bottom row: EHT 1864 (5 μM, 1hr).
(H) Quantification of cortical enrichment in CHO cells transfected with wild type Kv3.3 channels: actin (left) and Arp2/3 (right), control vs. EHT 1864 treatment (5 μM, 1hr); Parentheses: number cells measured, 3 measurements per cell; Values are mean ± SEM, *** $p < 0.001$, two-tailed unpaired t test.
See also Figure S2.

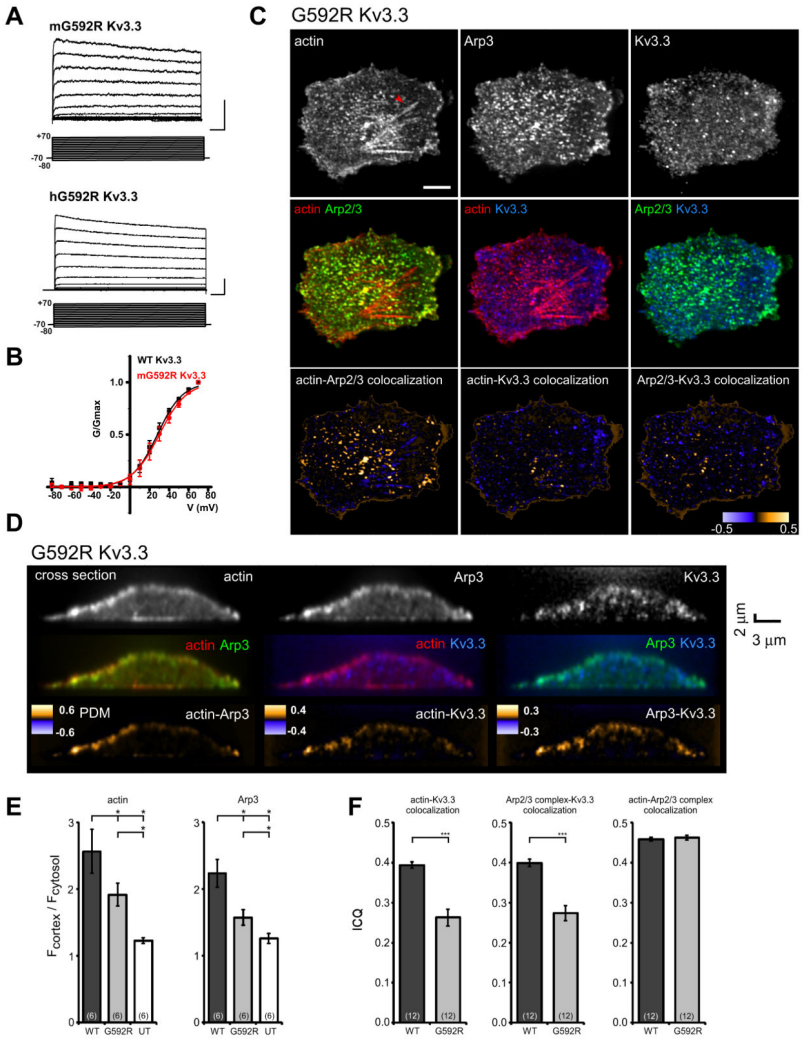

Figure 5. The G592R mutant Kv3.3 channel does not re-organize the actin cytoskeleton

(A) Representative mouse and human G592R Kv3.3 currents, 10 mV increments, Scale bars 1nA, 50 msec.

(B) Normalized G/Gmax curves for mouse wild type and G592R Kv3.3 currents. Values are mean ± SEM, n = 9.

(C-D) CHO cells transfected with G592R Kv3.3 labeled with Alexa 594 phalloidin, Arp3 antibody and Kv3.3 antibody after fixation. XY view (*C*) and XZ view (*D*): top row: actin (left), Arp3 (middle) or Kv3.3 (right) images; middle row: overlay of actin and Arp3 (left), actin and Kv3.3 (middle) or Arp3 and Kv3.3 (right) images; bottom row: PDM (the product of the differences from the mean) quantifying colocalization level between: actin vs. Arp3 (left), actin vs. Kv3.3 (middle) or Arp3 vs. Kv3.3 (right).

(E) Quantification of cortical enrichment in cells transfected with wild type or G592R Kv3.3 or untransfected cells (data for wild type Kv3.3 expressing cells and untransfected cells are from Fig. 1 for comparison): actin (*left*), Arp2/3 (*right*); n = 6 cells per condition, 3 measurements per cell; Data provided as mean +/− SEM, $p < 1 \times 10^{-8}$ with single factor ANOVA, and asterisk indicates significant difference using Tukey's HSD post hoc analysis.

(F) ICQ (intensity correlation quotient) in CHO cells transfected with wild type or G592R Kv3.3 to assess colocalization of: actin vs. Kv3.3 (left), Arp2/3 vs. Kv3.3 (middle) or actin vs. Arp2/3 (right); Parentheses: number cells measured. Values are mean ± SEM, *** $p < 0.001$, two-tailed unpaired t test.

See also Figures S2, S5 and Movies 1-3.

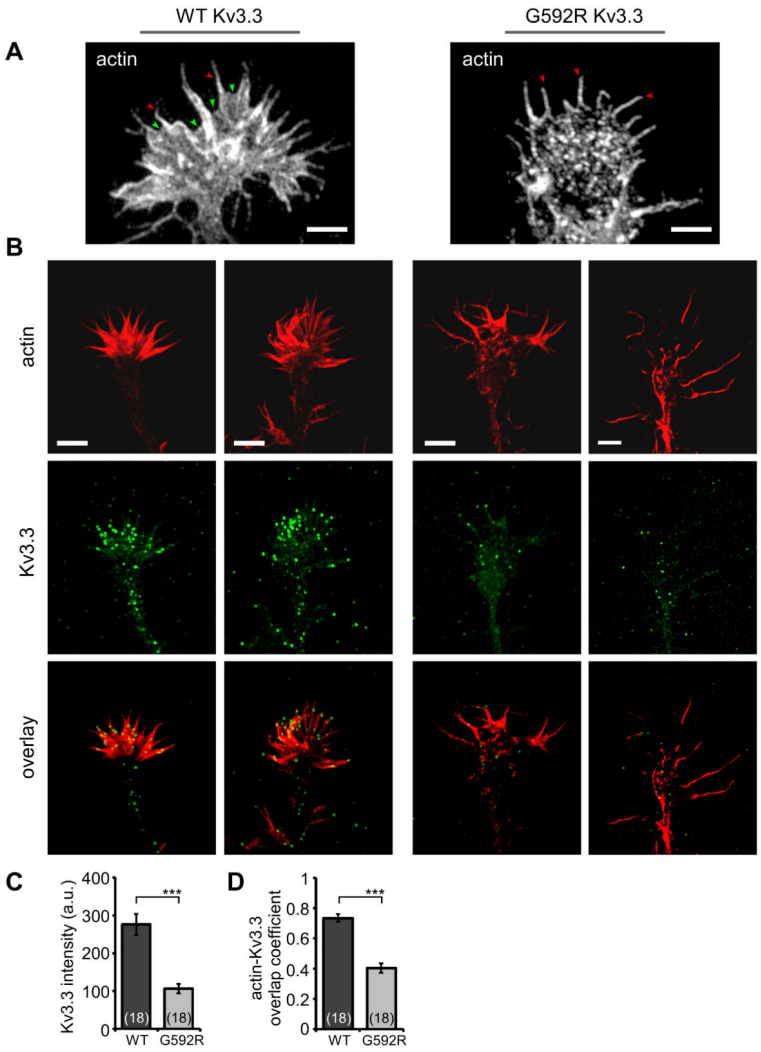

Figure 6. Localization of actin and Kv3.3 channels in neuronal cells derived from human iPS cells

(A) A neuronal growth cone derived from human wild type Kv3.3 iPSCs (left) or human G592R Kv3.3 iPSCs (right) labelled with Alexa 594 phalloidin to visualize actin filament structures; red and green arrow heads: filopodia and actin veils, respectively.

(B) Two representative examples of neuronal growth cones derived from human wild type Kv3.3 iPSCs (left, two columns) or human G592R Kv3.3 iPSCs (right, two columns) labeled with Alexa594 phalloidin and Kv3.3 antibody after fixation. Top row: actin; Middle row: Kv3.3; Bottom row: overlay of actin and Kv3.3; for Kv3.3, fluorescent intensity scales were constant between wild type Kv3.3 and G592R Kv3.3 growth cones; scale bar: 5 μm.

(C) Quantification of Kv3.3 fluorescent intensity in wild type Kv3.3 and G592R Kv3.3 neuronal growth cones. Parentheses indicate number growth cones measured; values are mean ± SEM, *** $p < 0.001$ two-tailed unpaired t test;

(D) Quantification of actin-Kv3.3 overlap coefficient in wild type Kv3.3 and G592R Kv3.3 neuronal growth cones. Parentheses indicate number growth cones measured; Values are mean ± SEM, *** $p < 0.001$, two-tailed unpaired t test.

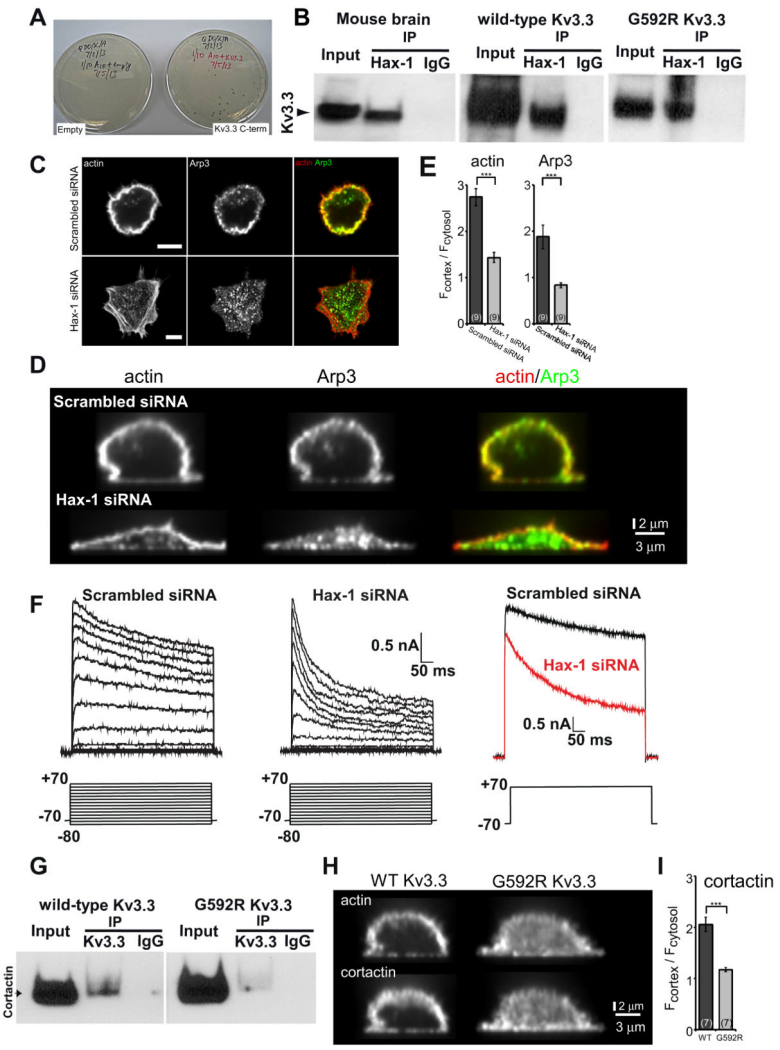

Figure 7. The C terminus of Kv3.3 interacts with Hax-1

(A) Confirmation of interaction between C-terminus of Kv3.3 (aa 542-769) and Hax-1 in yeast two hybrid screen. *Left:* control pairwise mating assay using yeast clone containing the Kv3.3 C-terminus and empty pGAD vector. *Right:* mating under stringent conditions of yeast clone transformed with human Hax-1 with yeast clone containing Kv3.3 C-terminus.
(B) Western blots demonstrating co-immunoprecipitation of Kv3.3 with Hax-1 from extracts of mouse cerebellum and CHO cells stably expressing wild-type Kv3.3 or G592R Kv3.3.
(C-D) Hax-1 siRNA treatment delocalizes cortical Arp2/3 in wild type Kv3.3 CHO cells. CHO cells treated with scrambled siRNA (top) or Hax-1 siRNA (bottom) labeled with Alexa 594 phalloidin and Arp3 antibody after fixation. *C* and *D*: XY and XZ views, respectively of: actin (left), Arp3 (middle) and overlay of actin and Arp3 (right).
(E) Quantification of cortical enrichment of actin and Arp3 in wild type Kv3.3 CHO cells treated with scrambled siRNA or Hax-1 siRNA; n = 9 cells per condition, 3 measurements per cell; Values are mean ± SEM *** $p < 0.001$, two-tailed unpaired t test.

(F) Representative voltage clamp currents in Kv3.3-expressing CHO cells 72 hrs after transfection with scrambled siRNAi (*left*) or siRNA directed against Hax-1 (*center*). Right panels show superimposed currents for the two treatments.
(G) Western blots demonstrating that cortactin co-immunoprecipitates with wild-type Kv3.3 channels (*left*) but less effectively with G592R Kv3.3 (*right*).
(H) G592R Kv3.3 channel expression reduces cortactin cortical localization. XZ view of CHO cells transfected with wild type Kv3.3 (left) or G592R Kv3.3 (right) labeled with Alexa594 phalloidin and cortactin antibody after fixation.
(I) Quantification of cortical enrichment of cortactin in CHO cells transfected with wild type or G592R Kv3.3; n = 7 cells per condition, 3 measurements per cell; Values are mean ± SEM, *** $p < 0.001$, two-tailed unpaired t test. See also Figures S6 and S7.